

Error compensation without a time penalty: robust spin-lock-induced crossing in solution NMR

Mohamed Sabba, Christian Bengs, Urvashi D. Heramun, and Malcolm H. Levitt*

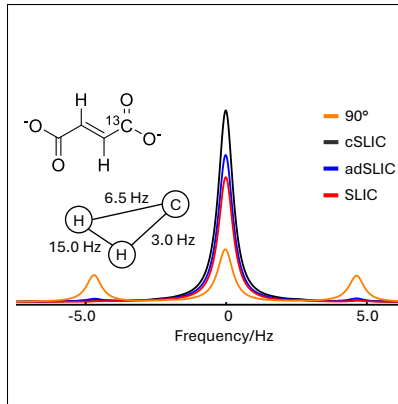
School of Chemistry and Chemical Engineering, University of Southampton, Southampton SO17 1BJ, UK

E-mail: mhl@soton.ac.uk

Abstract

A modification of the widely-used spin-lock-induced crossing (SLIC) procedure is proposed for the solution nuclear magnetic resonance (NMR) of strongly coupled nuclear spin systems, including singlet NMR and parahydrogen-enhanced hyperpolarised NMR experiments. The compensated-SLIC (cSLIC) scheme uses a repetitive sequence where the repeated element employs two different radiofrequency field amplitudes. Effective compensation for deviations in the radiofrequency field amplitude is achieved without increasing the overall duration of the SLIC sequence. The advantageous properties of cSLIC are demonstrated by numerical simulations and by representative experiments.

TOC Graphic



1. INTRODUCTION

The spin-lock-induced crossing (SLIC) method was introduced by De Vience *et al.* in 2013 as a simple method for generating long-lived singlet order for near-equivalent spin pairs in nuclear magnetic resonance.¹ SLIC involves the application of a resonant radiofrequency field with the same phase as transverse nuclear spin magnetisation. The amplitude of the resonant field is chosen so that the nutation frequency under the rf field matches the J-coupling between the members of the spin pair:

$$\omega_{\text{nut}} = \omega_J, \quad (1)$$

where $\omega_J = 2\pi J$. When applied to strongly coupled spin-1/2 pairs $|\omega_\Delta| \ll |\omega_J|$, where $\omega_\Delta = 2\pi\Delta$, and Δ is the chemical shift difference in units of Hz. This matching condition induces a level crossing in a suitable reference frame² which

leads to the coherent evolution of transverse magnetisation into nuclear singlet order (SO). Singlet order represents a net difference in populations of the singlet and triplet states of the spin-1/2 pair

$$Q_{\text{SO}} = |S_0\rangle\langle S_0| - \frac{1}{3} \sum_m |T_m\rangle\langle T_m| = -\frac{4}{3} \mathbf{I}_j \cdot \mathbf{I}_k, \quad (2)$$

where $|S_0\rangle$ and $|T_m\rangle$ are the singlet and triplet states formed by the two participating spins I_j and I_k .^{3,4} In suitable circumstances, singlet order is a “long-lived state”, protected against some common relaxation mechanisms, and which may exhibit a decay time constant exceeding 1 hour in favourable circumstances.⁵

SLIC has also been used for the selection of desirable NMR⁶ and MRI^{7,8} signals, the estimation of J-coupling differences on the order of a few mHz,⁹ for chemically infor-

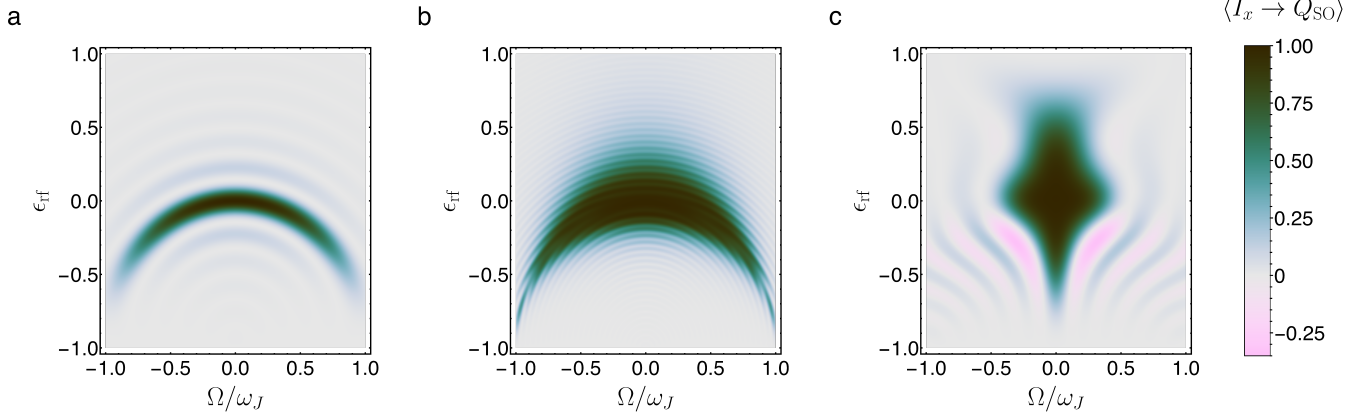


Figure 1: Contour plots for the transformation amplitude of transverse magnetisation into singlet order, defined by $\langle I_x \rightarrow Q_{\text{SO}} \rangle = \text{Tr}\{Q_{\text{SO}}U_I U^\dagger\}/\text{Tr}\{Q_{\text{SO}}Q_{\text{SO}}\}$, where U represents the propagator for a specific SLIC element. Results are shown for (a) SLIC, (b) adSLIC, (c) cSLIC against resonance offset (horizontal axis) and deviations in the rf amplitude (vertical axis). All simulations are performed for a two-spin system with $J = 15$ Hz and $\Delta = 1.9$ Hz. The total durations of the elements T are: 375 ms (SLIC and cSLIC) and 1560 ms (adSLIC) respectively. For cSLIC, the repetition number is $n = 6$ and $\alpha = 0.99$. For adSLIC, the rf-amplitude modulation is given by Equation 5 with $\Delta_{\text{max}} = 0.5$ and $\xi = 0.9$.

mative J-spectroscopy in low magnetic fields,^{10–12} and for parahydrogen-enhanced NMR.^{7,13–18} SLIC may also be used to manipulate multiple-quantum transitions in strongly coupled spin systems.^{19–23}

Many applications of SLIC are hampered by its high sensitivity to deviations in the rf field amplitude. This behaviour is illustrated by the contour plot in Fig. 1(a), which shows the amplitude for the transformation of transverse nuclear magnetisation (described by the operator I_x) into nuclear singlet order (described by the operator Q_{SO}). The transformation amplitude is plotted as a function of two parameters. The horizontal axis shows the J-coupling normalised resonance offset

$$\Omega = \Omega_{\text{rf}} - \frac{1}{2} \left(\Omega_j^0 + \Omega_k^0 \right), \quad (3)$$

where Ω_{rf} is the radio-frequency field frequency and Ω_j^0 , Ω_k^0 are the chemically-shifted Larmor frequencies of the two spins. The vertical axis shows the fractional deviation of the rf field amplitude, expressed as a nutation frequency, ω_{nut} , from the nominal value ω_{nut}^0 :

$$\epsilon_{\text{rf}} = \frac{\omega_{\text{nut}} - \omega_{\text{nut}}^0}{\omega_{\text{nut}}^0}. \quad (4)$$

The narrow crescent shape traced out by the contours in figure 1(a) indicate that the performance of SLIC is very sensitive to the rf amplitude when applied at exact resonance, and also that the resonance offset and rf amplitude errors interact strongly. In general, these are undesirable characteristics. In particular, the high rf field sensitivity implies a degradation in performance whenever the rf field is inhomogeneous over the sample volume, as is often the case.

Several methods have been proposed for rendering SLIC less sensitive to amplitude errors. One popular option is to extend the pulse sequence duration while varying the rf amplitude continuously so as to sweep through a range of matching conditions.^{24,25} This solution is often known as adiabatic-SLIC (adSLIC) even though the strict adiabaticity

conditions on the spin dynamics are not always met.^{25,26} Simulations for one possible amplitude shape given by Theis and coworkers^{24,27} are shown in figure 1(b), where the specific rf-amplitude modulation is given by:

$$\begin{aligned} \omega_{\text{nut}}(t) &= \omega_J [1 - \Delta_{\text{max}} \tan(x\xi\pi/2) / \tan(\xi\pi/2)], \\ x &= 2t/T - 1, \end{aligned} \quad (5)$$

where the time variable t runs from 0 to the total duration T . The parameter $-1 < \Delta_{\text{max}} < 1$ defines the size and direction of the sweep, whereas $0 < \xi < 1$ is a shape parameter, with small values of ξ converging to a linear sweep and large values leading to a more adiabatic transfer.

As expected, sensitivity to the rf amplitude is reduced relative to unmodulated SLIC, albeit at the cost of a significantly increased duration, which can lead to increased losses through dissipation, although this is not taken into account in the calculations of figure 1. In practice, this dissipation sets the ultimate limit on performance enhancement: while in principle, the robustness of adSLIC can be increased indefinitely by increasing the pulse duration, which is not possible in spin systems which relax rapidly. In the simulation of Figure 1(b), a total adSLIC duration of $T = 500$ ms was chosen, approximately seven times longer than the SLIC sequence, to ensure a fair comparison.

2. THE cSLIC SEQUENCE

We recently showed that SLIC may also be used for double-quantum excitation in systems of spin-1/2 pairs, and proposed a modified SLIC sequence, called compensated-SLIC or cSLIC, in order to improve its tolerance to errors.²⁸ The cSLIC sequence was shown to provide effective compensation for rf amplitude deviations, without an increase in pulse sequence duration relative to the uncompensated SLIC method. Here we show that the cSLIC sequence is also significantly more robust than uncompensated SLIC in the context of singlet NMR, and in contexts such as parahydrogen-enhanced NMR.

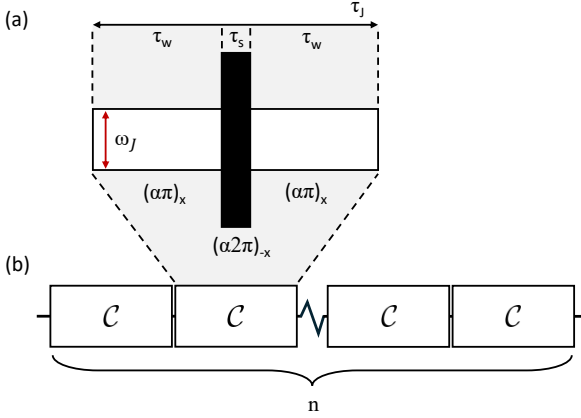


Figure 2: Pulse sequence schematic for cSLIC. (a) The basic element consists of a concatenation of two weak pulses separated by a strong pulse. The weak pulses are of amplitude $\omega_{\text{nut}}^{\text{weak}} = \omega_J$, duration τ_w and produce a net rotation of $(\alpha\pi)$ along the x -axis. The strong central pulse is of amplitude $\omega_{\text{nut}}^{\text{strong}} > \omega_J$, duration τ_s and produces a net rotation of $(\alpha 2\pi)$ along the $-x$ -axis. The parameter $\frac{1}{2} \leq \alpha \lesssim 1$ is defined by equation 8. The pulse durations are constrained by $2\tau_w + \tau_s = \tau_J$. (b) cSLIC-based singlet excitation consists of $n = \lfloor J/(\sqrt{2}\Delta) \rfloor$ repetitions of the basic element shown in (a).

The cSLIC sequence involves n repetitions of the cyclic element C sketched in figure 2(a), which has the form:

$$C = (\alpha\pi)_x^{\text{weak}} - (\alpha 2\pi)_{-x}^{\text{strong}} - (\alpha\pi)_x^{\text{weak}}. \quad (6)$$

Compared to conventional SLIC, the cSLIC sequence employs two different amplitude levels: a weak rf field, and a stronger rf field which provides a compensatory counter-rotation in the centre of each repeating element. The nutation frequency of the two weak outer pulses matches the SLIC condition:

$$\omega_{\text{nut}}^{\text{weak}} = \omega_J. \quad (7)$$

By contrast, the strong central pulse is assumed to have a nutation frequency that is much larger than those of the outer pulses, $\omega_{\text{nut}}^{\text{strong}} > \omega_{\text{nut}}^{\text{weak}}$. The parameter $\frac{1}{2} < \alpha \lesssim 1$ is given by

$$\alpha = \frac{\omega_{\text{nut}}^{\text{strong}}}{\omega_{\text{nut}}^{\text{strong}} + \omega_{\text{nut}}^{\text{weak}}}. \quad (8)$$

In the limit of an infinitesimally short central pulse ($\omega_{\text{nut}}^{\text{strong}} \gg \omega_{\text{nut}}^{\text{weak}}$), the parameter α tends to 1, and the cSLIC sequence becomes

$$\text{cSLIC}(\alpha \rightarrow 1) = (\pi)_x^{\text{weak}} - (2\pi)_{-x}^{\text{strong}} - (\pi)_x^{\text{weak}}, \quad (9)$$

where the central 2π pulse has negligible duration. In practice, this limit cannot be reached, due to hardware limitations, but it can be approached sufficiently closely.

The duration of each cSLIC element is given by $\tau_J = |J|^{-1}$ for all values of α . In the absence of relaxation, the singlet-order generation for an ensemble of 2-spin-1/2 systems is maximised when n is chosen as follows:²⁸

$$n = \lfloor J/(\sqrt{2}\Delta) \rfloor, \quad (10)$$

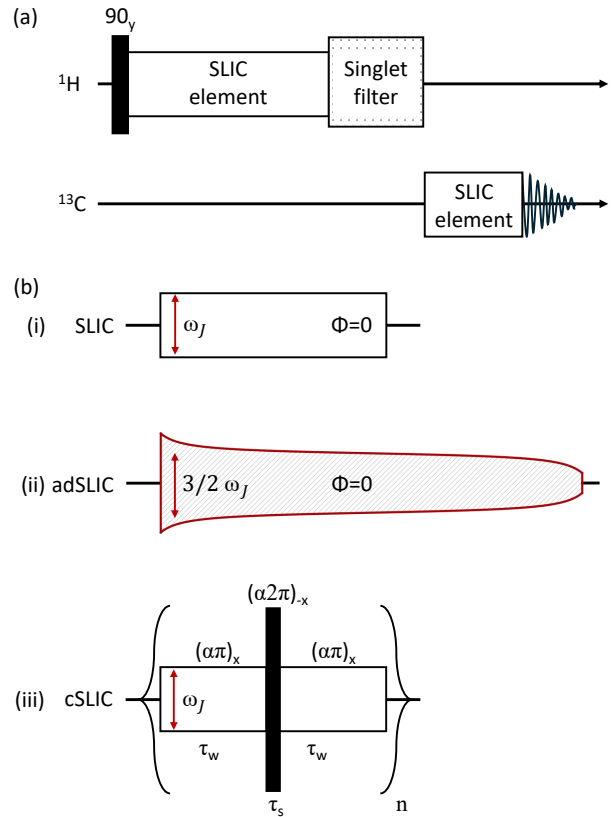


Figure 3: (a) Pulse sequence for heteronuclear polarization transfer from ^1H to ^{13}C , through an intermediate ^1H singlet state, in systems of two ^1H nuclei and one ^{13}C nucleus, as in figure 4. An initial 90°_y pulse generates transverse proton magnetisation, followed by a singlet preparation element using one of the SLIC variants shown in (b). After singlet-order preparation, a filter element removes any spurious density-operator terms. A second SLIC variant transforms singlet order into heteronuclear magnetisation. (b) SLIC elements used in this work. (i) The basic SLIC element consists of a single x pulse with amplitude ω_J . (ii) Adiabatic SLIC consists of an amplitude-modulated x pulse following the functional form given in Equation 5. (iii) The cSLIC element follows the procedure outlined in fig. 2.

where $\lfloor x \rfloor$ rounds x to its nearest integer.

The compensation principle can be illustrated in the limit $\alpha = 1$, where the duration of the central compensating pulse is negligible compared to the element duration τ_J . Assume that the sequence is applied on-resonance ($\Omega = 0$). Under these ideal conditions, the two weak SLIC pulses combine to generate a 2π rotation, and the central pulse generates an equal and opposite 2π rotation. When the rf field amplitude of the weak pulses is larger than expected, $\omega_{\text{nut}}^{\text{weak}} = (1 + \epsilon_{\text{rf}})\omega_J$, the excess rotation induced by the misset SLIC field is compensated by the equal and opposite excess rotation caused by the misset strong pulse – and similarly when the rf field is weaker than nominal. This compensation mechanism assumes that the weak and strong rf fields experience the rf amplitude errors in the same proportion. This is the case when both fields are generated by the same radiofrequency coil, and when the deviations are caused by spatial variations in the rf field strength. This is the usual experimental situation.

If the central pulse strength does not dominate the outer

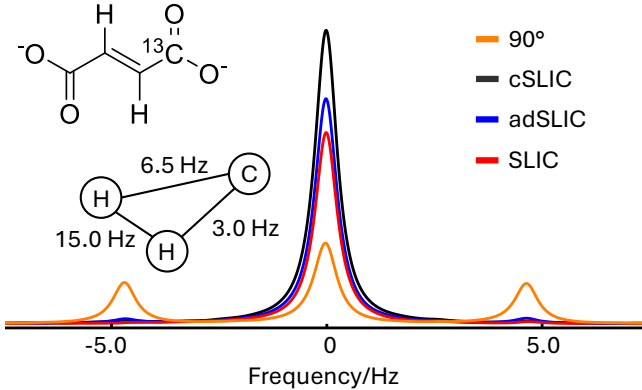


Figure 4: ^{13}C spectra of $[1-^{13}\text{C}]\text{-fumarate}$ dissolved in D_2O . Inset shows the chemical structure and the J-coupling parameters. Fourier transform (green) of the free-induction decay generated by a single 90° ^{13}C pulse applied to a sample in thermal equilibrium. ^{13}C spectra for SLIC (pink), adSLIC (blue), and cSLIC (black) were obtained using the pulse sequence strategy shown in Figure 3. 0.5 Hz of line broadening was applied to all spectra. The pulse sequence parameters are summarised in the experimental details.

pulses ($\alpha < 1$), the net rotations of the inner and outer pulses still compensate each other for any value of the overall rf amplitude, and the duration of each repeating element still matches one period τ_J of the J-coupling frequency. Hence, the basic physics of the level anticrossing^{2,14,29} still applies, albeit with slightly reduced state-mixing coefficients. The simulation shown in figure 1(c) confirms this analysis for the realistic case $\alpha = 0.99$. The robustness of the singlet excitation amplitude with respect to rf amplitude deviations is greatly improved, at the expense of a somewhat reduced frequency bandwidth. The undesirable interaction between rf amplitude and resonance offset effects is strongly reduced. The improved error compensation of cSLIC is achieved with the same sequence duration as uncompensated SLIC.

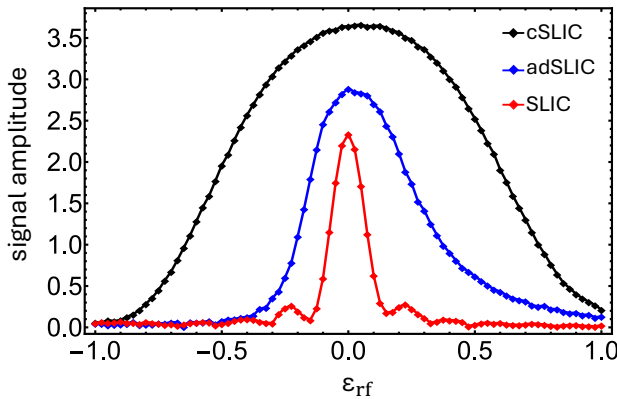


Figure 5: Experimental ^{13}C signal amplitude for singlet-mediated heteronuclear polarisation transfer in $[1-^{13}\text{C}]\text{-fumarate}$, as a function of the fractional ^{13}C nutation amplitude mismatch, defined in Equation 4. Signal amplitudes have been normalised against the amplitude of the central peak in the 90° spectrum.

3. EXPERIMENTAL DETAILS

The experimental performance of the SLIC, adSLIC, and cSLIC sequences was evaluated by performing singlet-mediated heteronuclear polarization transfer experiments on a solution of $[1-^{13}\text{C}]\text{-fumarate}$ in D_2O . The heteronuclear pulse sequence scheme shown in Fig. 3(a) was used. This has previously been employed to evaluate SLIC and related methods in the context of parahydrogen-enhanced ^{13}C NMR.¹⁵ Although the two ^1H nuclei in $[1-^{13}\text{C}]\text{-fumarate}$ are chemically equivalent, they have different J-couplings with the ^{13}C nucleus. This J-coupling difference effectively takes the role of the chemical shift difference in spin-1/2 pairs,^{15,30} allowing generation of ^1H singlet order from ^1H transverse magnetisation when a ^1H -SLIC sequence is applied. The J-coupling difference also allows the conversion of ^1H singlet order into ^{13}C transverse magnetisation when a subsequent SLIC sequence is applied on the ^{13}C channel. In the absence of dissipation, the optimal duration of the second SLIC pulse is shorter than that of the first SLIC pulse, by a factor of $\sqrt{2}$ (see ref. ¹⁵).

Experiments were performed on a 200 mM solution of $[1-^{13}\text{C}]\text{-fumarate}$ in D_2O at a magnetic field of 9.4 T. The pulse powers were adjusted to provide a nutation frequency of 25.0 kHz on the ^{13}C channel and 10.0 kHz on the ^1H channel, corresponding to 90° pulse durations of 10 μs and 25 μs , respectively. The pulse sequence in figure 3(a) deploys a standard singlet filtration sequence^{31,32} in order to suppress any ^{13}C NMR signals that do not pass through ^1H singlet order between the two SLIC sequences. The experimentally optimised parameters for the sequences were $\{T_{\text{H}}, T_{\text{C}}\} = \{524 \text{ ms}, 370 \text{ ms}\}$ (SLIC), $\{T_{\text{H}}, T_{\text{C}}, n_{\text{H}}, n_{\text{C}}, \alpha\} = \{500 \text{ ms}, 381 \text{ ms}, 8, 6, 0.988\}$ (cSLIC), and $\{T_{\text{H}}, T_{\text{C}}, \Delta_{\text{max}}, \xi\} = \{1780 \text{ ms}, 1560 \text{ ms}, 0.5, 0.9\}$ (adSLIC), and $\omega_J/(2\pi) = 15 \text{ Hz}$.

4. RESULTS

Figure 4(orange) shows a ^{13}C spectrum of $[1-^{13}\text{C}]\text{-fumarate}$ solution generated by a 90° ^{13}C pulse applied to the sample in thermal equilibrium. ^1H decoupling was not applied. The ^{13}C spectrum shows a triplet multiplet structure due to the J-couplings of the ^{13}C nucleus to the two fumarate ^1H nuclei, which are nearly magnetically equivalent due to the large J_{HH} coupling, the relatively small difference between the two J_{CH} couplings, and the very small difference in chemical shifts between the two ^1H sites.¹⁵

Figure 4(red) shows a ^{13}C spectrum obtained by generating ^1H singlet order using a conventional ^1H SLIC sequence of duration $T_{\text{H}} = 524 \text{ ms}$, suppressing any other density operator components by a singlet filter sequence, and applying a conventional ^{13}C SLIC sequence of duration $T_{\text{C}} = 370 \text{ ms}$ to generate transverse ^{13}C magnetisation. The signal intensity is enhanced relative to that in Figure 4(orange), since the ^1H singlet order is generated from thermal-equilibrium ^1H magnetisation, which is approximately four times larger than that of ^{13}C . The outer multiplet components of the ^{13}C signal are suppressed, as expected by theory.¹⁵

Figure 4(blue) shows a ^{13}C spectrum of $[1-^{13}\text{C}]\text{-fumarate}$ obtained under identical conditions, but using adSLIC sequences for both of the SLIC elements in figure 3. The

adSLIC elements followed the functional form given in Equation 5 and had overall durations of $T_H = 1780$ ms and $T_C = 1560$ ms, with $\Delta_{\max} = 0.5$, $\xi = 0.9$ in both cases. The spectrum shown in Figure 4(blue) was obtained after a sincere attempt to optimise the adSLIC shape parameters on both channels; longer durations led to a deterioration of the performance. In this case, only a moderate improvement is evident over the fixed-amplitude SLIC result in Figure 4(red).

Figure 4(black) shows the ^{13}C spectrum obtained when using cSLIC for both SLIC elements of the pulse sequence. The parameters used were $T_H = 500$ ms, $T_C = 381$ ms, $n_H = 8$, $n_C = 6$, and $\alpha = 0.988$. The spectrum obtained with cSLIC shows a significantly stronger signal than that achieved with both SLIC and adSLIC.

Figure 5 demonstrates the experimental response of the three methods to rf amplitude variations. In all cases the amplitudes of the strong and weak pulses were kept in the same fixed ratio. SLIC displays poor compensation against rf field errors. Deviations as small as $\pm 10\%$ in the rf amplitude reduce the polarization transfer amplitude by $\sim 50\%$. adSLIC displays considerable more robustness with respect rf amplitude deviations, especially on the high-amplitude side. In contrast, cSLIC remains largely unaffected by modest rf field variations, retaining half of its peak efficiency even for fractional errors as large as $\pm 50\%$. The enhanced amplitude of cSLIC over SLIC and adSLIC, as shown in Fig. 4, may thus be attributed to the substantially reduced sensitivity of cSLIC to rf field amplitude variations across the sample volume.

CONCLUSIONS

This work demonstrates that cSLIC provides markedly improved compensation against RF field deviations, as compared to SLIC and adSLIC, retaining high singlet-order transfer efficiencies even under substantial nutation amplitude mismatches. Although not demonstrated explicitly, this enhanced robustness makes cSLIC particularly attractive for parahydrogen-induced polarisation (PHIP) applications, where maximising heteronuclear polarisation transfer is critical for achieving practical levels of hyperpolarisation. Importantly, cSLIC achieves these advantages as a relatively low-power method: although the central pulse is referred to here as “strong”, it needs to be only modestly more intense than the conventional SLIC element; typically around five times the SLIC field is sufficient. Counterintuitively, the error-compensation is achieved without increasing the overall sequence duration, in contrast to composite pulse²⁴ or optimal control variants of SLIC which are power-efficient but have a lengthened duration.³³ The method is also fully compatible with magic-angle (MA) compensation schemes for dipolar field effects, which are important for attaining high molar polarisation in PHIP applications.^{18,34} Additionally, as shown in Section II of the Supporting Information, the performance of the cSLIC sequence can be further enhanced through supercycling, an option that is not readily available for the other methods, and may even be used for DNP. Collectively, these features should make cSLIC a practical tool for enhancing experimental transfer efficiencies in a wide range of NMR experiments exploiting nuclear singlet states and similar phenomena.

AUTHOR CONTRIBUTIONS

Mohamed Sabba: Conceptualization (lead), Methodology (lead), Investigation (lead), Data Curation (lead), Software (lead), Visualization (equal), Writing - original draft (equal), Writing - review & editing (equal)

Christian Bengs: Visualization (lead), Writing - original draft (lead), Writing - review & editing (lead)

Urvashi D. Heramun: Conceptualization (equal)

Malcolm H. Levitt: Conceptualization (equal), Funding acquisition (lead), Supervision (lead), Writing - original draft (equal), Writing - review & editing (equal)

CONFLICTS OF INTEREST

MS has received consulting fees from Synex Medical. The other authors have no conflicts to declare.

DATA AVAILABILITY

The data that support the findings of this study are available from the corresponding author, MS, upon reasonable request.

ACKNOWLEDGEMENTS

We acknowledge funding from the European Research Council (Grant No. 786707-FunMagResBeacons) and EPSRC-UK (Grant Numbers EP/P030491/1, EP/V047663/1, EP/V055593/1, and EP/V047663/1). We acknowledge Matthew S. Rosen and Stephen J. DeVience for sharing valuable insights on the SLIC sequence, and Nino Wili for pointing out similarities with the NOVEL sequence.

SUPPORTING INFORMATION

The supporting information contains brief details of the theory for multiple use cases of the (c)SLIC sequence, and simulations of supercycled variants of cSLIC.

REFERENCES

- DeVience, S. J.; Walsworth, R. L.; Rosen, M. S. Preparation of Nuclear Spin Singlet States Using Spin-Lock Induced Crossing. *Physical Review Letters* **2013**, *111*, 173002.
- Rodin, B. A.; Ivanov, K. L. Representation of Population Exchange at Level Anti-Crossings. *Magnetic Resonance* **2020**, *1*, 347–365.
- Levitt, M. H. Singlet Nuclear Magnetic Resonance. *Annual Review of Physical Chemistry* **2012**, *63*, 89–105.
- Levitt, M. H. Long Live the Singlet State! *Journal of Magnetic Resonance* **2019**, *306*, 69–74.
- Stevanato, G.; Hill-Cousins, J. T.; Håkansson, P.; Roy, S. S.; Brown, L. J.; Brown, R. C. D.; Pileio, G.; Levitt, M. H. A Nuclear Singlet Lifetime of More than One Hour in Room-Temperature Solution. *Angewandte Chemie* **2015**, *127*, 3811–3814.
- DeVience, S. J.; Walsworth, R. L.; Rosen, M. S. NMR of ^{31}P Nuclear Spin Singlet States in Organic Diphosphates. *Journal of Magnetic Resonance* **2021**, *333*, 107101.
- Boele, T.; McBride, S. J.; Pike, M.; Curran, E.; TomHon, P.; Braaksma, H.; Shen, S.; Koonjoo, N.; Korenchan, D. E.; Chekmenev, E. et al. Ultra-Low Field ^{13}C MRI of Hyperpolarized Pyruvate. 2025.

(8) McBride, S. J.; Pike, M.; Curran, E.; Zavriyev, A.; Adebessin, B.; Tucker, L.; Harzan, J. M.; Senanayake, I. M.; Abdulmojeed, M.; Theiss, F. et al. Scalable Hyperpolarized MRI Enabled by Ace-SABRE of [1-13C]Pyruvate. *Angewandte Chemie International Edition* **2025**, *64*, e202501231.

(9) DeVience, S. J.; Walsworth, R. L.; Rosen, M. S. Probing Scalar Coupling Differences via Long-Lived Singlet States. *Journal of Magnetic Resonance* **2016**, *262*, 42–49.

(10) DeVience, S. J.; Greer, M.; Mandal, S.; Rosen, M. S. Homonuclear J-Coupling Spectroscopy at Low Magnetic Fields Using Spin-Lock Induced Crossing. *ChemPhysChem* **2021**, *22*, 2128–2137.

(11) DeVience, S. J.; Rosen, M. S. Homonuclear J-coupling Spectroscopy Using J-synchronized Echo Detection. *Journal of Magnetic Resonance* **2022**, *341*, 107244.

(12) Mandzhieva, I.; Theiss, F.; He, X.; Ortmeier, A.; Koirala, A.; McBride, S. J.; DeVience, S. J.; Rosen, M. S.; Blum, V.; Theis, T. Zero-Field NMR and Millitesla-SLIC Spectra for >200 Molecules from Density Functional Theory and Spin Dynamics. *Journal of Chemical Information and Modeling* **2025**, *65*, 7554–7568.

(13) Theis, T.; Truong, M.; Coffey, A. M.; Chekmenev, E. Y.; Warren, W. S. LIGHT-SABRE Enables Efficient in-Magnet Catalytic Hyperpolarization. *Journal of Magnetic Resonance* **2014**, *248*, 23–26.

(14) Pravdivtsev, A. N.; Yurkovskaya, A. V.; Vieth, H.-M.; Ivanov, K. L. Spin Mixing at Level Anti-Crossings in the Rotating Frame Makes High-Field SABRE Feasible. *Physical Chemistry Chemical Physics* **2014**, *16*, 24672–24675.

(15) Eills, J.; Stevanato, G.; Bengs, C.; Glöggler, S.; Elliott, S. J.; Alonso-Valdesueiro, J.; Pileio, G.; Levitt, M. H. Singlet Order Conversion and Parahydrogen-Induced Hyperpolarization of ¹³C Nuclei in near-Equivalent Spin Systems. *Journal of Magnetic Resonance* **2017**, *274*, 163–172.

(16) Knecht, S.; Kiryutin, A. S.; Yurkovskaya, A. V.; Ivanov, K. L. Efficient Conversion of Anti-Phase Spin Order of Protons into ¹⁵N Magnetisation Using SLIC-SABRE. *Molecular Physics* **2019**, *117*, 2762–2771.

(17) Sheberstov, K. F.; Kozinenko, V. P.; Kiryutin, A. S.; Vieth, H.-M.; Zimmermann, H.; Ivanov, K. L.; Yurkovskaya, A. V. Hyperpolarization of Cis-15N2-Azobenzene by Parahydrogen at Ultralow Magnetic Fields. *ChemPhysChem* **2021**, *22*, 1527–1534.

(18) Dagys, L.; Korzeczek, M. C.; Parker, A. J.; Eills, J.; Blanchard, J. W.; Bengs, C.; Levitt, M. H.; Knecht, S.; Schwartz, I.; Plenio, M. B. Robust Parahydrogen-Induced Polarization at High Concentrations. *Science Advances* **2024**, *10*, eado0373.

(19) Sonnenfeld, A.; Bodenhausen, G.; Sheberstov, K. Polychromatic Excitation of Delocalized Long-Lived Proton Spin States in Aliphatic Chains. *Physical Review Letters* **2022**, *129*, 183203.

(20) Sonnenfeld, A.; Razanahoera, A.; Pelupessy, P.; Bodenhausen, G.; Sheberstov, K. Long-Lived States of Methylen Protons in Achiral Molecules. *Science Advances* **2022**, *8*, eade2113.

(21) Sheberstov, K. F.; Sonnenfeld, A.; Bodenhausen, G. Collective Long-Lived Zero-Quantum Coherences in Aliphatic Chains. *The Journal of Chemical Physics* **2024**, *160*, 144308.

(22) Razanahoera, A.; Sonnenfeld, A.; Sheberstov, K.; Narwal, P.; Minaei, M.; Kouřil, K.; Bodenhausen, G.; Meier, B. Hyperpolarization of Long-Lived States of Protons in Aliphatic Chains by Bullet Dynamic Nuclear Polarization, Revealed on the Fly by Spin-Lock-Induced Crossing. *The Journal of Physical Chemistry Letters* **2024**, *15*, 9024–9029.

(23) Wiame, C.; Van Dyck, S.; Sheberstov, K.; Razanahoera, A.; Bodenhausen, G. Long-Lived States Involving a Manifold of Fluorine-19 Spins in Fluorinated Aliphatic Chains. *Magnetic Resonance* **2025**, *6*, 273–279.

(24) Theis, T.; Feng, Y.; Wu, T.; Warren, W. S. Composite and Shaped Pulses for Efficient and Robust Pumping of Disconnected Eigenstates in Magnetic Resonance. *The Journal of Chemical Physics* **2014**, *140*, 014201.

(25) Rodin, B. A.; Sheberstov, K. F.; Kiryutin, A. S.; Hill-Cousins, J. T.; Brown, L. J.; Brown, R. C. D.; Jamain, B.; Zimmermann, H.; Sagdeev, R. Z.; Yurkovskaya, A. V. et al. Constant-Adiabaticity Radiofrequency Pulses for Generating Long-Lived Singlet Spin States in NMR. *The Journal of Chemical Physics* **2019**, *150*, 064201.

(26) Comparat, D. General Conditions for Quantum Adiabatic Evolution. *Physical Review A* **2009**, *80*, 012106.

(27) Clayton, K. E. Making Nuclear Magnetic Hyperpolarization Practical through Storage in Disconnected Eigenstates. Ph.D. thesis, Duke University, United States – North Carolina, 2015.

(28) Heramun, U.; Sabba, M.; Yamano, D.; Bengs, C.; Legrady, B.; Thompson, S.; Pileio, G.; Levitt, M. H. Spinor Double-Quantum Excitation in the Solution NMR of Near-Equivalent Spin-1/2 Pairs. *Journal of Chemical Physics* **2026**, *in press*.

(29) Pravdivtsev, A. N.; Yurkovskaya, A. V.; Kaptein, R.; Miesel, K.; Vieth, H.-M.; Ivanov, K. L. Exploiting Level Anti-Crossings for Efficient and Selective Transfer of Hyperpolarization in Coupled Nuclear Spin Systems. *Physical Chemistry Chemical Physics* **2013**, *15*, 14660–14669.

(30) Korzeczek, M. C.; Dagys, L.; Müller, C.; Tratzmiller, B.; Salhov, A.; Eichhorn, T.; Scheuer, J.; Knecht, S.; Plenio, M. B.; Schwartz, I. Towards a Unified Picture of Polarization Transfer — Pulsed DNP and Chemically Equivalent PHIP. *Journal of Magnetic Resonance* **2024**, *362*, 107671.

(31) Tayler, M. C. D. *Long-Lived Nuclear Spin Order: Theory and Applications*; New Developments in NMR; 2020.

(32) Harbor-Collins, H.; Sabba, M.; Bengs, C.; Moustafa, G.; Leutzsch, M.; Levitt, M. H. NMR Spectroscopy of a ¹⁸O-labeled Rhodium Paddlewheel Complex: Isotope Shifts, ¹⁰³Rh–¹⁰³Rh Spin–Spin Cou-

pling, and ^{103}Rh Singlet NMR. *The Journal of Chemical Physics* **2024**, *160*, 014305.

(33) Goodwin, D. L. Advanced Optimal Control Methods for Spin Systems. Ph.D. thesis, University of Southampton, 2017.

(34) Korzeczek, M. C.; Schwartz, I.; Plenio, M. B. PHIP Sequences and Dipolar Fields. 2025.

Error compensation without a time penalty: robust spin-lock-induced crossing in solution NMR

Mohamed Sabba,^{1, a)} Christian Bengs,¹ Urvashi Heramun,¹ and Malcolm H. Levitt¹

*Department of Chemistry, University of Southampton, SO17 1BJ,
UK*

(Dated: February 10, 2026)

^{a)}Electronic mail: m.sabba@soton.ac.uk

I. BASIC THEORY OF SLIC

A. Single transition operators

In order to rationalize SLIC and cSLIC by effective Hamiltonian theory, it is appropriate to define single-transition operators^{1,2}. A set of single-transition operators for the subspace of the two arbitrary states $|\alpha\rangle$ and $|\beta\rangle$ could be written as:

$$\begin{aligned} I_x^{\alpha,\beta} &= \frac{1}{2} (|\alpha\rangle\langle\beta| + |\beta\rangle\langle\alpha|) \\ I_y^{\alpha,\beta} &= \frac{1}{2i} (|\alpha\rangle\langle\beta| - |\beta\rangle\langle\alpha|) \\ I_{\phi}^{\alpha,\beta} &= \cos(\phi) I_x^{\alpha,\beta} + \sin(\phi) I_y^{\alpha,\beta} \\ I_z^{\alpha,\beta} &= \frac{1}{2} (|\alpha\rangle\langle\alpha| - |\beta\rangle\langle\beta|) \\ \mathbb{1}^{\alpha,\beta} &= |\alpha\rangle\langle\alpha| + |\beta\rangle\langle\beta| \end{aligned} \quad (1)$$

B. The effective Hamiltonian of SLIC in an AB spin system

The singlet and triplet states of an isolated spin-1/2 pair are defined as follows:

$$\begin{aligned} |S_0\rangle &= (|\alpha\beta\rangle - |\beta\alpha\rangle)/\sqrt{2}, \\ |T_+\rangle &= |\alpha\alpha\rangle, \\ |T_0\rangle &= (|\alpha\beta\rangle + |\beta\alpha\rangle)/\sqrt{2}, \\ |T_-\rangle &= |\beta\beta\rangle \end{aligned} \quad (2)$$

And the Hamiltonian of this spin system, H_{AB} , can be expressed like so:

$$H_{AB} = H_{\Delta} + H_J \quad (3)$$

$$H_{\Delta} = \omega_{\Delta}(I_{1z} - I_{2z})/2 = \omega_{\Delta}I_x^{T_0, S_0} \quad (4)$$

$$H_J = \omega_J I_1 I_2 = \omega_J \left(I_z^{T_0, S_0} + I_{1z} I_{2z} \right) \quad (5)$$

Where $\omega_J = 2\pi J_{12}$ represents the J-coupling and $\omega_{\Delta} = 2\pi\Delta$ represents the chemical shift difference $\Delta = v_0^1 - v_0^2$.

A key realization is that in the strongly coupled regime ($J_{12} \gg \Delta$), H_{Δ} should be understood as the *driving interaction*, whereas H_J plays the role of the strong *modulating term* that appears in pulse sequences as a matching condition.

Suppose that the SLIC sequence is defined as follows:

$$\text{SLIC}_\pm(\tau) = (\pi/2)_{-y} - [\text{SL}]_{\pm x}^{\omega_{\text{nut}}=\omega_J}(\tau) - (\pi/2)_{+y} \quad (6)$$

Where $[\text{SL}]_{\phi}^{\omega_{\text{nut}}=\omega_J}(\tau)$ denotes spin-locking of duration τ , phase ϕ , and nutation frequency ω_J .

The final pulse is not necessary at all for the operation of the sequence, but has been inserted to simplify the theory by avoiding working in a tedious tilted frame.

We now evaluate \tilde{H}_Δ , the interaction frame Hamiltonian that describes the SLIC sequence, for both positive ($+x$) and negative ($-x$) senses of continuous-wave irradiation:

$$\begin{aligned} \tilde{H}_\Delta(\tau) &= \exp\left[+i\frac{\pi}{2}I_{-y}\right] \exp\left[+i\theta_J(I_1I_2 \pm I_x)\right] H_\Delta \exp\left[-i\theta_J(I_1I_2 \pm I_x)\right] \exp\left[-i\frac{\pi}{2}I_{-y}\right] \\ &= \mp\sqrt{2}\pi\Delta\left(I_x^{S_0,T_\pm} - I_{\omega_J\tau}^{S_0,T_\mp}\right) \end{aligned} \quad (7)$$

And proceed to calculate the effective Hamiltonian $\overline{H}_{\text{SLIC}_\pm}^{(1)}$ over a cycle corresponding to a full J -period $T = 1/J$:

$$\begin{aligned} \overline{H}_{\text{SLIC}}^{(1)} &= \frac{1}{T} \int_0^T \tilde{H}_\Delta(\tau) d\tau, \quad T = 1/J \\ &= \mp\sqrt{2}\pi\Delta I_x^{S_0,T_\pm} \end{aligned} \quad (8)$$

The most critical point here is that the mechanism of the SLIC sequence can be fully explained by the above effective Hamiltonian, which engineers a transition between the state $|S_0\rangle$ and either of the triplet states $|T_\pm\rangle$, depending on the phase of the SLIC pulse. We now proceed to "translating" this picture to other applications of SLIC.

C. Other contexts where SLIC (and cSLIC) are applicable

Rather than derive multiple effective Hamiltonians for the various different situations in which SLIC (and analogous sequences such as NOVEL) are applicable on a case-by-case basis, we find it more convenient to provide a table containing a list of relevant transitions $|r\rangle \leftrightarrow |s\rangle$, rf amplitude matching conditions (or resonances) in terms of the modulation frequency Ω_μ , and driving terms characterized by a Rabi frequency ω_u .

| Sequence | Transition | Matched rf amplitude (ω_{rf}) | Driving term [Rabi frequency, ω_{μ}] | Modulating term [Resonant frequency, Ω_{μ}] |
|---------------|--|--|--|--|
| SLIC (AB) | $ S_0\rangle \leftrightarrow T_{\pm}\rangle$ | ω_{nut}^{12} | chemical shift difference [$\sqrt{2}\pi\Delta$] | J-coupling [$2\pi J_{12}$] |
| SLIC (PHIP) | $ \alpha^S S_0^L\rangle \leftrightarrow \beta^S T_{\pm}^I\rangle$ | ω_{nut}^S | differential coupling [$\pi(J_{IS} - J_{I'S})/2$] | homonuclear J-coupling [$2\pi J_{II}$] |
| SLIC (AA'XX') | $ T_{\pm}^A S_0^X\rangle \leftrightarrow S_0^A T_0^X\rangle$ | ω_{nut}^A | out-of-pair coupling difference [$\pi(J_{AX} - J_{AX'})/\sqrt{2}$] | in-pair coupling (difference) [$2\pi(J_{AA} - J_{XX'})$] |
| SLIC (AA'XX') | $ T_{\pm}^A T_0^X\rangle \leftrightarrow S_0^A S_0^X\rangle$ | ω_{nut}^A | out-of-pair coupling difference [$\pi(J_{AX} - J_{AX'})/\sqrt{2}$] | in-pair coupling (sum) [$2\pi(J_{AA} + J_{XX'})$] |
| NOVEL | $ \alpha^e \beta^n\rangle \leftrightarrow \beta^e \alpha^n\rangle$ or $ \alpha^e \alpha^n\rangle \leftrightarrow \beta^e \beta^n\rangle$ | ω_{nut}^e | electron-nuclear coupling [$\pi J_{\text{en}}/2$] | nuclear Larmor frequency [ω_0^n] |

Table SI. A table of various analogues of the SLIC pulse sequence. All sequences are fully characterized by their particular target transitions, the matching condition $\omega_{\text{rf}} = \Omega_{\mu}$ relating a nutation frequency to the modulation frequency Ω_{μ} , and driving terms which allow population transfer with a Rabi frequency ω_{μ} .

D. Generalized response of SLIC to rf amplitude errors

In the most general case, the dependence of the excitation efficiency of SLIC on rf amplitude errors ϵ_{rf} corresponds to the familiar textbook case of a detuned Rabi oscillation:

$$\xi_{\text{SLIC}}(t) = \sin^2(\theta_{\mu}) \sin^2 \left(\frac{1}{2} \omega_{\mu} \csc(\theta_{\mu}) t \right) \quad (9)$$

Where the "detuning angle" θ_{μ} is defined in terms of the Rabi frequency ω_{μ} and the effective detuning frequency Ω_{μ} :

$$\theta_{\mu} = \arctan \left(\frac{\omega_{\mu}}{\Omega_{\mu} \epsilon_{\text{rf}}} \right) \quad (10)$$

For a nominal duration $t = \pi/\omega_\mu$ the efficiency is simply:

$$\xi_{\text{SLIC}}(\pi/\omega_\mu) = \frac{\pi^2}{4} \text{sinc}^2\left(\frac{\pi}{2} \csc(\theta_\mu)\right) \quad (11)$$

Which is a narrowband sinc-squared response, depicted in Figure S1. The extreme sensitivity of the SLIC sequence (and analogues such as NOVEL) to the matching condition presents a major source of inconvenience to the variety of experiments mentioned beforehand.

E. The effective Hamiltonian of the cSLIC sequence in an AB spin system

The effective Hamiltonian of the cSLIC sequence, as shown in the appendix of another reference³, is given by the following in the limit of a negligibly short compensating pulse ($\alpha \rightarrow 1$):

$$\begin{aligned} \bar{H}_{\text{cSLIC}}^{(1)} &= \lim_{\alpha \rightarrow 1} \int_0^{1/J} \tilde{H}_\Delta(t) \, dt \\ &= -\sqrt{2}\pi\Delta[\text{sinc}(f_+) I_x^{S_0, T_+} - \text{sinc}(f_-) I_x^{S_0, T_-}] \end{aligned} \quad (12)$$

where the arguments of the sinc functions are:

$$\begin{aligned} f_+ &= \pi\epsilon_{\text{rf}} \\ f_- &= \pi(2 + \epsilon_{\text{rf}}) \end{aligned} \quad (13)$$

These represent a pair of counter-rotating frequency components, centred at the resonances of the two nominal SLIC matching conditions: $\omega_{\text{nut}}^{\text{SLIC}} = +\omega_J$ ($\epsilon_{\text{rf}} = 0$), and $\omega_{\text{nut}}^{\text{SLIC}} = -\omega_J$ ($\epsilon_{\text{rf}} = -2$).

F. Generalized response of cSLIC as a function of rf amplitude errors

In the most general case, the excitation efficiency of cSLIC is given by the following function:

$$\xi_{\text{cSLIC}}(t) = \frac{f_-^2 - f_+^2}{f_-^2 + f_+^2} \sin^2\left(\frac{1}{2}\omega_\mu \sqrt{\text{sinc}^2(f_-) + \text{sinc}^2(f_+)} t\right) \quad (14)$$

When compared to Equation 9, the dependence on the Ω_μ term has vanished. The dependence on ϵ_{rf} is solely due to interference between the two matching conditions f_- and f_+ .

For a nominal duration $t = \pi/\omega_\mu$, the excitation efficiency of cSLIC becomes:

$$\xi_{\text{cSLIC}}(t = \pi/\omega_\mu) = \frac{f_-^2 - f_+^2}{f_-^2 + f_+^2} \sin^2\left(\frac{\pi}{2} \sqrt{\text{sinc}^2(f_-) + \text{sinc}^2(f_+)}\right) \quad (15)$$

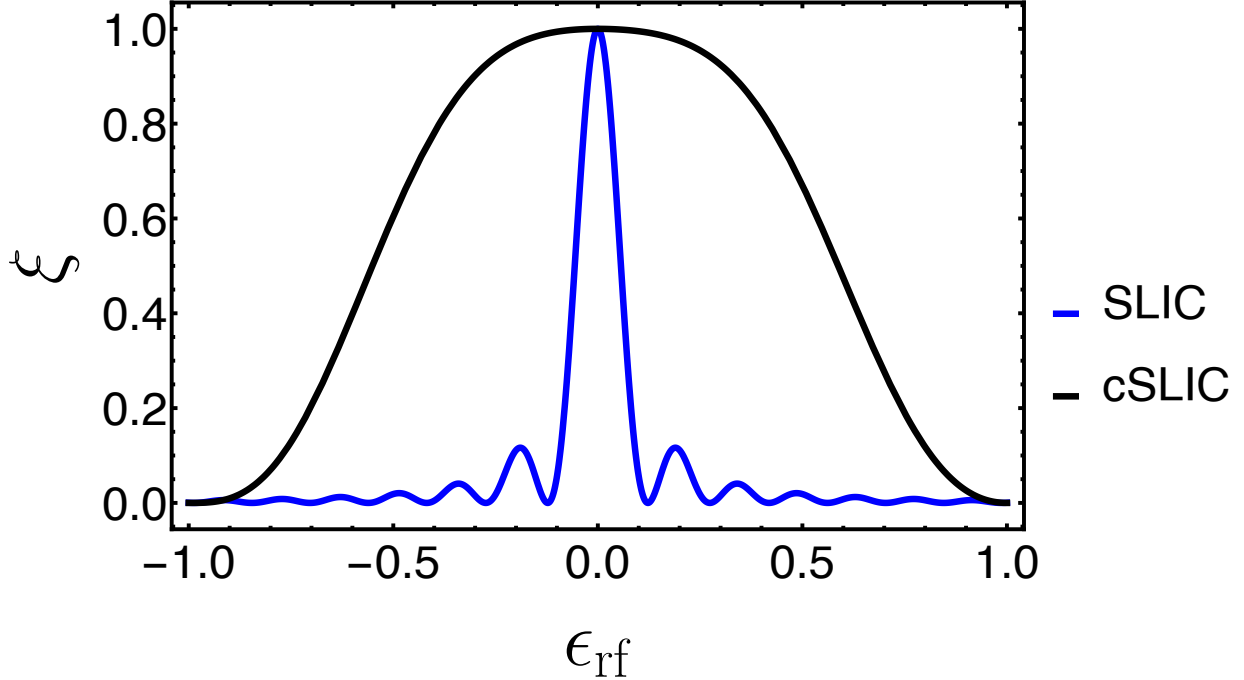


Figure S1. Analytical excitation efficiencies ξ of the SLIC and cSLIC sequences as a function of rf amplitude error ϵ_{rf} , using equations 11 and 15. The parameters used for SLIC are the Rabi frequency $\omega_\mu = \omega_\Delta/\sqrt{2}$ and $\Omega_\mu = \omega_J$, with $\omega_\Delta = 2\pi \times 10$ and $\omega_J = 2\pi \times 100$.

A comparison of the analytical equations describing the rf error dependence of SLIC (equation 11) and cSLIC (equation 15) is shown in Figure S1. The cSLIC sequence (or what would be the analogous "cNOVEL" sequence in the context of DNP) has a broadband response whereas the SLIC sequence has a narrowband response that worsens for larger values of Ω_μ/ω_μ .

II. SUPERCYCLED VARIANTS OF cSLIC

\mathcal{C} , the cyclic element building block of the cSLIC pulse sequence used in this paper, can be expressed in terms of the two inversion elements A and B:

$$\begin{aligned} A &= 180_x^{\omega_{\text{nut}}=\omega_J} \\ B &= 180_{-x}^{\omega_{\text{nut}}=\omega_{\text{strong}}} \end{aligned} \quad (16)$$

The position of the compensating pulse element "BB" is not particularly important; it may be placed at the beginning, middle, or end of the pulse sequence without affecting the performance,

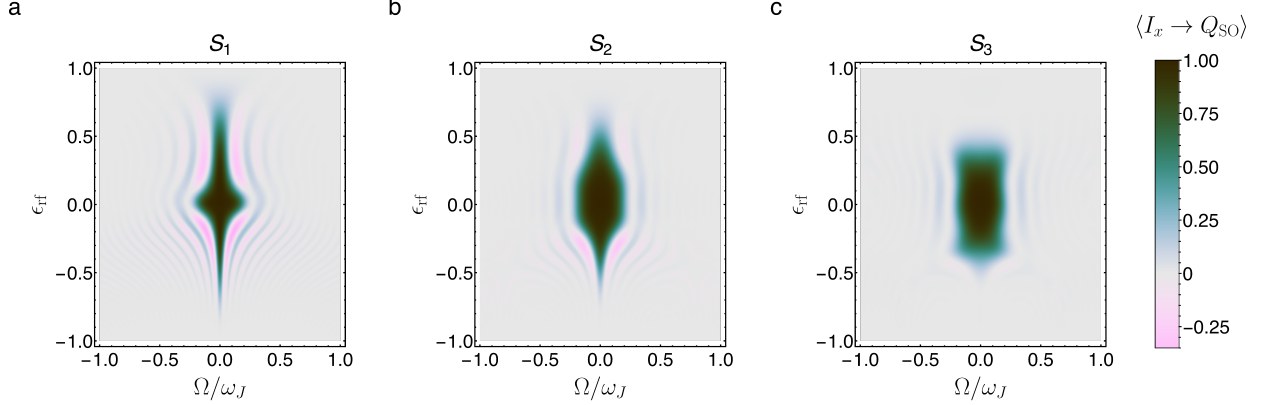


Figure S2. Numerical simulations showing the performance of supercycled variants of cSLIC as a function of rf amplitude errors ϵ_{rf} and relative resonance offset errors Ω/ω_J . Panel (a): the primitive cycle $S_1 = \text{ABBA}$. Panel (b): the 8-step supercycle $S_2 = \text{AABBABBA}$. Panel (c): the 12-step supercycle $S_3 = \text{AABBABBABBAA}$. The simulations are performed for a 2-spin-1/2 system with $\omega_J = 2\pi \times 100$, and $\omega_\Delta = 2\pi \times 3$, assuming $\alpha = 0.99$.

and indeed all of the following cyclic elements may be used to compose the cSLIC sequence:

$$\mathcal{C}_1 = \text{AABB} \quad (17)$$

$$\mathcal{C}_2 = \text{ABBA} \quad (18)$$

$$\mathcal{C}_3 = \text{BBA} \quad (19)$$

The variant of cSLIC used in this paper (ABBA) was chosen purely for aesthetic reasons, and as a tribute to the Swedish pop band that bears the same moniker.

Combining the different permutations C_i can be used to improve the performance of cSLIC as a function of resonance offset, at the expense of increased sensitivity to rf amplitude errors. For example, some "supercycles"^{4,5} with better off-resonance performance (denoted S_i) are:

$$\begin{aligned} S_1 &= \mathcal{C}_2 \\ S_2 &= \mathcal{C}_1 \mathcal{C}_2 \\ S_3 &= \mathcal{C}_1 \mathcal{C}_2 \mathcal{C}_3 \end{aligned} \quad (20)$$

The performance of these supercycled variants is shown in Figure S2. The S_3 variant of cSLIC shows more uniform performance, with no generation of negative singlet order, at the expense of a smaller on-resonance ϵ_{rf} bandwidth.

REFERENCES

¹A. Wokaun and R. R. Ernst, Journal of Chemical Physics **67**, 1752 (1977).

²S. Vega, The Journal of Chemical Physics **68**, 5518 (1978).

³U. Heramun, M. Sabba, D. Yamano, C. Bengs, B. Legrady, S. Thompson, G. Pileio, and M. H. Levitt, Journal of Chemical Physics **in press** (2026).

⁴D. P. Burum, M. Linder, and R. R. Ernst, Journal of Magnetic Resonance (1969) **44**, 173 (1981).

⁵M. H. Levitt, The Journal of Chemical Physics **128**, 052205 (2008).